

Online Humidity and Temperature Decorrelation of Chemical Sensors for Continuous Monitoring

Ramon Huerta¹, Thiago Mosqueiro¹, Jordi Fonollosa², Nikolai F Rulkov¹ and Irene Rodriguez-Lujan³

1 BioCircuits Institute, University of California San Diego, La Jolla, USA

2 Institute for Bioengineering of Catalunya, Baldiri Reixac 4-8, 08028 Barcelona, Spain

3 Dpto. de Ingeniería Informática, Escuela Politécnica Superior, Universidad Autónoma de Madrid, Calle Francisco Tomás y Valiente, 11, 28049 Madrid, Spain

Abstract

A method for online decorrelation of chemical sensor readings from the effects of environmental humidity and temperature variations is proposed. The goal is to improve the accuracy of electronic nose measurements for continuous monitoring by processing data from simultaneous readings of environmental humidity and temperature. The electronic nose setup built for this study included eight different metal-oxide sensors, temperature and humidity sensors with a wireless communication link to PC. This wireless electronic nose was used to monitor air for two years in the residence of one of the authors and collected data continuously during 510 full days with a sampling rate of 2 samples per second. To estimate the effects of variations in air humidity and temperature on the chemical sensors readings, we used a standard energy band model for an n-type metal-oxide sensor. The main assumption of the model is that variations in sensor conductivity can be expressed as a nonlinear function of changes in the semiconductor energy bands in the presence of external humidity and temperature variations. Fitting this model to the collected data, we confirmed that the most statistically significant factors are humidity changes and correlated changes of temperature and humidity. This simple model achieves excellent accuracy with R^2 performance close to 1. To show how the humidity-temperature correction model works for gas discrimination, we also collected 100 samples of wine and banana. The goal is to distinguish between wine, banana, and baseline. We show that pattern recognition algorithms improve performance and reliability by including the filtered signal of the chemical sensors.

Keywords: electronic nose, chemical sensors, humidity, temperature, decorrelation, wireless e-nose, MOX sensors, energy band model, home monitoring

1 Introduction

Conductometric chemical sensors are known to be very sensitive to humidity levels in the environment [1, 2, 3, 4, 5, 6, 7, 8, 9, 10, 11]. This sensitivity challenges the tasks of identification and quantification of volatiles in uncontrolled scenarios. For example, electronic noses can be used for human monitoring purposes [12, 13, 14, 15, 16, 17]. They have been successfully used to quantify the number of people working in a space-craft simulator [18]. It is likely that the

primary signal used by the algorithm to estimate the number of people present at some given time is the humidity levels in the chamber. If we filter the sensor responses by the humidity and temperature changes, a clearer chemical signature of the chamber can be obtained, and this can facilitate more complex monitoring tasks like detecting individuals. A possible solution to this sensitivity problem is a design of a special sensing chamber that controls humidity and delivers the gas to the sensors under predefined conditions [19, 20, 21, 18, 8]. Such preconditioning chambers are effective for signal improvement, but their use increases the costs of electronic nose design for applications in continuous monitoring of the environment [14]. A different approach is to build a model that predicts the changes in the sensor conductance as a function of humidity and temperature variations [5, 8, 22, 23].

The prevailing phenomenological model of sensor sensitivity is that the ratio of the sensor resistance depends on a power law of the gas concentration [24]. The model provides accurate predictions when the gas is known and under controlled conditions. However, it is rendered inaccurate with changes in the environment. Correction methods based on artificial neural networks [8] using present and past values of the input features are proven to be successful despite lacking an explanation of the underlying processes. Fundamental models, on the other hand, can capture the dynamical changes of resistance under humidity variations accurately [22]. The number of parameters is not large, but the model parameters depend on the gas presented to the sensors. In continuous monitoring systems, there can be a complex mixture of gases present in the air. Thus, it is indeed challenging to make proper corrections on the sensor readings based on humidity and temperature variations.

In Fig. 1 we show a representative example of the humidity problem using chemical sensors for continuous monitoring purposes. The electronic nose in our setup utilizes 8 metal oxide (MOX) sensors and temperature and humidity sensors. Such platform was previously used in our wind tunnel studies to identify 10 gases at different locations [25]. As a result of this previous investigation, we know that we can discriminate between gases accurately, and estimate gas concentrations in the ppm range [26]. A fragment of recordings presented in Fig. 1 were obtained in October 2014 in a regular working day, in the residence of one of the authors. The top panel shows the humidity levels throughout a complete day where the x -axis indicates the hour of the day. For example, the first rise in humidity at about 5:30AM corresponds to the morning shower. The sudden drop in humidity at about 6:30 AM indicates opening the bathroom window, and the change observed at 5PM is associated with the moment at which the family came back and the door to the backyard was opened. The second panel presents the temperature of the electronic nose location that we denote by T_E to differentiate it from the temperature of the sensor heater, T . This residence did not have any air conditioning system or heater operating during this period. One can see from this graph that the environmental changes in humidity and temperature in some time intervals are correlated, while in other intervals are not correlated. The resistance values of the MOX sensors are presented in the four bottom panels. Although the sensor board is made of 8 MOX sensors, here we present recordings of only 4 of them because the remaining sensors are highly correlated with the shown ones. The resistance plots show that humidity and temperature changes strongly affect the resistance of the sensors as expected from the extensive literature on the topic [1, 2, 3, 4, 5, 6, 7, 8, 9, 10, 11]. Nevertheless, the data include also MOX sensor variations that are not a result of the humidity or T_E variations. Our goal is to subtract the humidity and temperature driven changes from the MOX sensor responses, and demonstrate that pattern recognition algorithms benefit from this operation augmenting its ability to discriminate

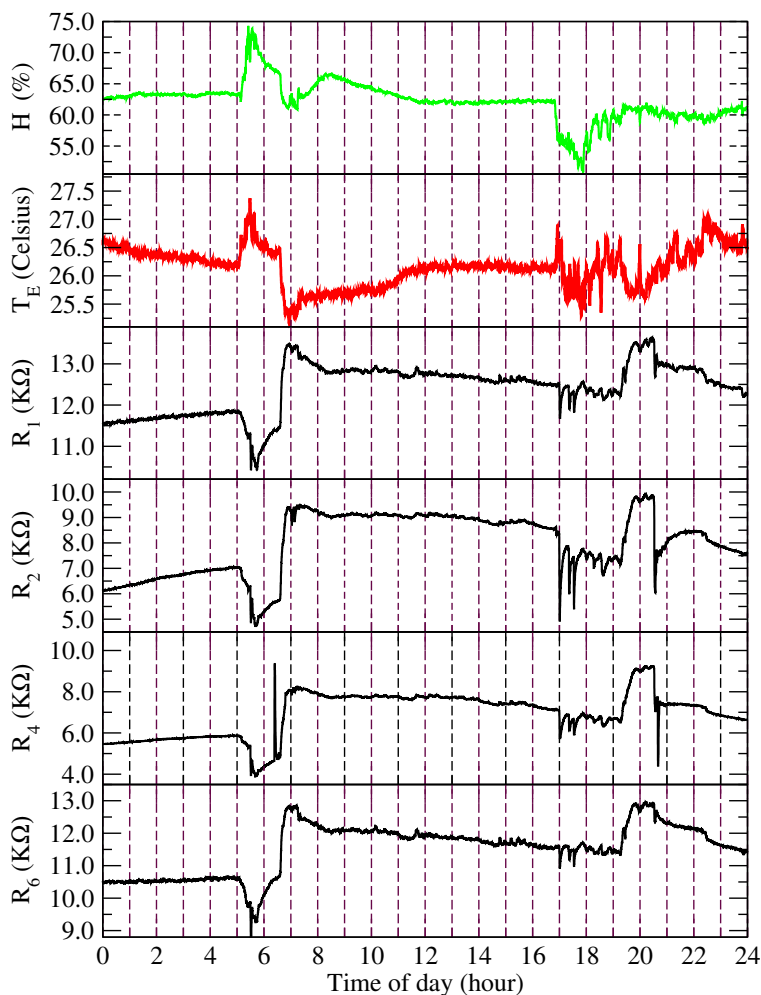


Figure 1: Illustrative example of one full day of recordings using the wireless electronic nose made of 8 MOX sensors including a humidity and temperature sensor. The first panel presents the humidity values, the second panel is the external temperature, and then resistance values for 4 different MOX sensors in the board. The x -axis is the hour of the day for a total of 24 hours.

different chemical signatures. We test it by creating a dataset of wine and banana, and solve the problem of identifying whether the sensor signal was banana, wine or baseline at different times of the day. This is a crucial task for any electronic nose system if one wants to characterize or detect events based on their chemical signatures in the presence of varying environmental conditions.

The paper starts with the section explaining the model used in our method, followed by the description of the wireless electronic nose used in experiments and the main section presenting the results. In the results section, we analyze the relationship of the parameters of the model fit to the data with the energy band model. Then, we analyze the stability of the parameters over time to determine how long the time window of the data is necessary. We also analyze the maximum sampling period to collect data from the electronic nose to be able to correct for humidity and temperature changes.

2 Model

An energy band model for n-type semiconductors describes the changes in the resistance of the sensor before exposure, R_I , and after exposure, R_F , as a nonlinear expression of the changes in the semiconductor's energy bands [1, 2]. Energy bands changes depend on variations in humidity and gas external temperature, which modulates the overall transduction. If we denote by $\Delta\Phi = \Phi_F - \Phi_I$ the work function change computed as the difference between the work function after and before exposure, and we express the electron affinity change as $\Delta\chi = \chi_F - \chi_I$, the overall transduction can be expressed (following [2]) as:

$$\ln\left(\frac{R_F}{R_I}\right) = \frac{1}{k_B T} (\Delta\Phi - \Delta\chi), \quad (1)$$

where k_B is the Boltzman constant, and T is the sensor operating temperature controlled by the built-in sensor heater. The sensor temperature is not constant because it is modulated by the external temperature, T_E . To be able to build a basic model to be fitted to the data, we make the following assumptions. We will assume that relative changes in the external humidity, $\Delta H = h$, and changes in external temperature, $\Delta T_E = t$, are small enough. We will also assume that during the environmental changes the chemical content remains unchanged. This is important because it is known that humidity changes induce nonlinear changes in the energy depending on the chemical agent (see [4]). Under these assumptions, we can rewrite the transduction equation 1 as

$$\ln\left(\frac{R_F}{R_I}\right) = \frac{1}{k_B(T + \mu t)} (\Delta\Phi(h) - \Delta\chi(h)), \quad (2)$$

where μ is a dimensionless factor that reflects the impact of the external temperature into the sensor. The sensor board based on the Texas Instruments MSP430F247 micro-controller can apply simple mathematical operations, so we want to make the corrections as linear as possible (see Fig. 2 in the following section). Thus, we apply a series expansion up to order 2 to avoid oversimplification:

$$\ln\left(\frac{R_F}{R_I}\right) = \left(\frac{1}{k_B T} - \frac{\mu}{k_B T^2} t + \frac{\mu^2}{k_B T^3} t^2 + O(t^3)\right) \times \left(\Delta\Phi(0) - \Delta\chi(0) + \left[\frac{\partial\Delta\Phi}{\partial h}\Big|_{h=0} - \frac{\partial\Delta\chi}{\partial h}\Big|_{h=0}\right] h + \frac{1}{2} \left[\frac{\partial^2\Delta\Phi}{\partial h^2}\Big|_{h=0} - \frac{\partial^2\Delta\chi}{\partial h^2}\Big|_{h=0}\right] h^2 + O(h^3)\right). \quad (3)$$

Note that $\Delta\Phi(0) - \Delta\chi(0) = 0$ because there are not changes in humidity and temperature on our sampling time scale. Then, we can simplify Equation (3) by considering terms up to order 2, assuming that the sampling period is small enough retaining the terms $h^i \cdot t^j$, with $i + j \leq 2$. In the results section, we will investigate the validity of this approximation. The simplified model is

$$\ln\left(\frac{R_F}{R_I}\right) = \frac{1}{k_B T} \left[\frac{\partial\Delta\Phi}{\partial h}\Big|_{h=0} - \frac{\partial\Delta\chi}{\partial h}\Big|_{h=0}\right] h + \frac{1}{2k_B T} \left[\frac{\partial^2\Delta\Phi}{\partial h^2}\Big|_{h=0} - \frac{\partial^2\Delta\chi}{\partial h^2}\Big|_{h=0}\right] h^2 - \frac{\mu}{k_B T^2} \left[\frac{\partial\Delta\Phi}{\partial h}\Big|_{h=0} - \frac{\partial\Delta\chi}{\partial h}\Big|_{h=0}\right] ht. \quad (4)$$

Therefore, we fit the following model to the data

$$\ln\left(\frac{R_F}{R_I}\right) = \beta_1 \Delta H + \beta_2 (\Delta H)^2 + \beta_3 \Delta H \Delta T_E, \quad (5)$$

Sensor type	Number of units	Target gases
TGS2611	1	Methane
TGS2612	1	Methane, Propane, Butane
TGS2610	1	Propane
TGS2600	1	Hydrogen, Carbon Monoxide
TGS2602	2	Ammonia, H2S, Volatile Organic Compounds (VOC)
TGS2620	2	Carbon Monoxide, combustible gases, VOC

Table 1: Sensor devices selected for the wireless electronic nose (provided by Figaro Inc.)

where

$$\begin{aligned}
\beta_1 &= \frac{1}{k_B T} \left[\frac{\partial \Delta \Phi}{\partial h} \Big|_{h=0} - \frac{\partial \Delta \chi}{\partial h} \Big|_{h=0} \right] \\
\beta_2 &= \frac{1}{2k_B T} \left[\frac{\partial^2 \Delta \Phi}{\partial h^2} \Big|_{h=0} - \frac{\partial^2 \Delta \chi}{\partial h^2} \Big|_{h=0} \right] \\
\beta_3 &= -\frac{\mu}{k_B T^2} \left[\frac{\partial \Delta \Phi}{\partial h} \Big|_{h=0} - \frac{\partial \Delta \chi}{\partial h} \Big|_{h=0} \right].
\end{aligned}$$

The main question is to verify how well the model can approximate our 500 days of data. In particular, this model predicts that the coefficients β_1 and β_3 have opposite sign and they are related by $\beta_3/\beta_1 = -\frac{\mu}{T}$. This means that the ratio $|\beta_3/\beta_1|$ becomes smaller with increasing sensor temperature. An empirical approach can be found in [23], where the model is fitted to a linear dependence on T_E and H , but not on the changes of the temperature and humidity.

3 Wireless electronic nose

In this section, we describe the electronic nose designed for home monitoring purposes. The sensor array is based on eight metal oxide gas sensors provided by Figaro Inc. The sensors are based on six different sensitive surfaces, which are selected to enhance the system selectivity and sensitivity. Table 1 shows the selected sensing elements along with the corresponding target compounds. In order to control the variability between the sensing elements and increase the flexibility of the sensing platform, the operating temperature of the sensors can be adjusted by applying a voltage to the built-in, independently reachable heating element available in each sensor. The humidity and temperature sensors are integrated in the board using the Sensirion SHT75. The device is very similar to the M-Pod [23], except that ours is directly powered by any electrical outlet to record continuously over long periods of time.

The sensor array is integrated with a customized board that includes a microprocessor MSP430F247 (Texas Instruments Inc.). In Fig. 2 we show the operating electronic nose. The microcontroller was programmed to perform the following actions: i) Continuous data collection from the eight chemical sensors through a 12-bit resolution analog-to-digital converter (ADC) device at a sampling rate of 100 Hz; ii) Control of the sensor heater temperature by means of 10 ms period and 6 V amplitude Pulse-Width-Modulated (PWM) driving signals; iii) A two-way communication with another device to transmit the acquired data from the sensors and control the voltage in

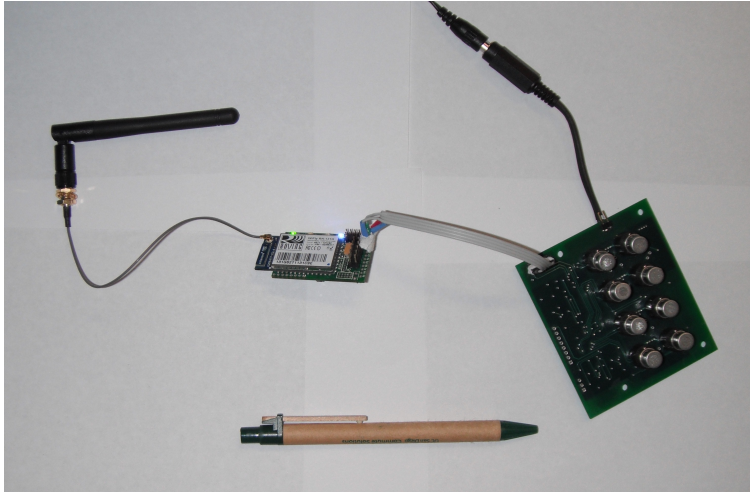


Figure 2: The electronic nose made of the sensor board (right) and a wireless communication board.

the sensors' heaters. The sensor board provides serial data communication to another device via either a USB and/or a 4-pin connector (Tx, Rx, Gnd, Vcc).

A wireless communication module acts as a bridge between the MSP430F247 microcontroller and the network. The communication with the MSP430F247 microcontroller is done via the UART port, whereas the communication with the network is performed wirelessly. The board is based on a WiFly RN-131G radio module included in a RN-134 SuRF board (Roving Networks Inc). The WiFly module incorporates a 2.4GHz radio, processor, full TCP/IP stack, real-time clock, FTP, DHCP, DNS and web server.

The module can be accessed via a RS-232 serial port (9600 default baud rate) or a 802.11 wireless network so that its configuration can be modified. The wireless communication module is configured such that it accepts UDP and TCP connections, the baudrate of the microprocessor is set to 115200 so that it can exchange data with the MSP430F247 microcontroller, and working with an external 4" reverse polarity antenna to increase the power of the transmission.

4 Results

We fit the model in equation (5) to the 537 days of data measured from Feb 17, 2013 till June 5 2015. To fit the model, we down-sample the time series to make only one data point per sensor every minute. Heaters for sensors 1-4 are always kept at the same operating voltage, while sensors 4 to 8 are controlled under a protocol that modifies the voltage (temperature) when some arbitrary conditions are achieved. Table 2 shows that the R^2 values of the fitted functions are remarkably close to 1, which is the best possible performance. All β parameters have very high statistical significance with p -values well below 10^{-10} . Moreover, as predicted by equation (4), the parameters β_1 and β_3 have opposite signs for all the sensors in the electronic nose. The β_3/β_1 ratios for the eight MOX sensors on the board are $-2.61, -2.21, -2.18, -2.19, -1.54, -1.84, -1.36,$ and -0.52 , which is consistent with an increasing voltage applied to the sensor's heater. The larger the voltage applied to the heater, the larger the temperature of the sensor.

Sensor	RMS	R^2	$\beta_1 (\beta_1/se(\beta_1))$	$\beta_2 (\beta_2/se(\beta_2))$	$\beta_3 (\beta_3/se(\beta_3))$
1	0.06	1.00	-0.0044 (-128.14)*	0.00014 (38.40)*	0.0110 (58.41)*
2	0.12	1.00	-0.0110 (-186.04)*	0.00034 (54.11)*	0.0240 (71.75)*
3	0.12	1.00	-0.0110 (-187.12)*	0.00034 (53.57)*	0.0230 (69.60)*
4	0.14	1.00	-0.0110 (-190.95)*	0.00033 (55.31)*	0.0230 (73.06)*
5	1.24	0.98	-0.0056 (-41.48)*	0.00018 (12.23)*	0.0086 (11.15)*
6	0.48	0.99	-0.0039 (-104.94)*	0.00012 (30.29)*	0.0071 (33.71)*
7	2.06	0.90	-0.0070 (-99.24)*	0.00022 (28.94)*	0.0095 (23.57)*
8	2.09	0.91	-0.0057 (-70.75)*	0.00020 (22.94)*	0.0029 (6.43)*

Table 2: Results of fitting model (5) to 739,479 data samples. RMS stands for root mean square, R^2 stands for the coefficient of determination such that the maximum value is 1, and $se()$ is the standard error of the parameter. The accuracy rates achieved are embodied in R^2 , which takes almost the maximum value for sensors 1 to 4. The accuracy is slightly worse for actively controlled sensors than for the first four sensors, but it is still very close to 1. That is, the approximation in equation (3) is not as good when the heater temperature is actively changed. All the parameters passed a test for statistical significance. p -values for all the factors are well below 10^{-10} (indicated with *). These results are extremely significant. Finally, note that according to the model, coefficients β_1 and β_3 have opposite signs for all the sensors. These results reveal that the energy band model fits well with the sensors of the electronic nose.

To filter the signal component proceeding from changes in humidity and temperature, we subtract the model output from the current raw sensor output. This operation is recognized as a method that searches signals independent of environmental conditions [27]. This is typically the case for continuously monitoring devices that are not intended to measure the concentration of a particular gas. The resulting signal is

$$R_i^*(t) = R_i(t) - \bar{R}_i(t) = R_i(t) - R_i(t-1)e^{(\beta_{1i}\Delta H + \beta_{2i}(\Delta H)^2 + \beta_{3i}\Delta H\Delta T_E)},$$

where R_i denotes the resistance values of the sensor i . In Fig. 3 we show the result of applying this transformation. On the left panel, we present the humidity, temperature, and sensor output. After applying the transformation, the decorrelated output of the sensor is shown on the right panel. The sensor drift due to the temperature and humidity changes is filtered out. However, we lose the relationship between the sensors when the stimulus is present which is typically gas-dependent [25].

4.1 Parameter Stability

To test the stability of the parameters over time, we train the model over a short period of time of 3 months of data and test its performance in the following month. Sometimes the electronic nose stopped transmitting due to wireless connections problems, or displaced from its location during house cleaning. There are many possible reasons in daily operations that can prevent the electronic nose from operating properly. Algorithms need to be as robust as possible given the uncontrolled conditions under which they can operate.

Testing the model with a 3 month window is quite strict because there are obviously seasonal changes in the environmental conditions along the year. Furthermore, the MOX sensors undergo

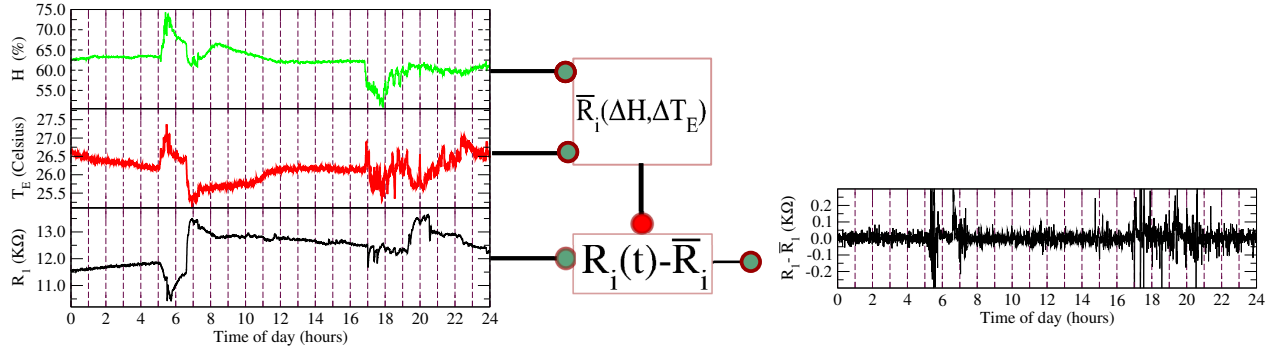


Figure 3: Result of applying the humidity and temperature filter provided by equation (5) on the first sensor. Humidity and temperature variations are used to estimate the current value of resistance of the sensor. This model output is subtracted from the original signal to obtain a filtered one.

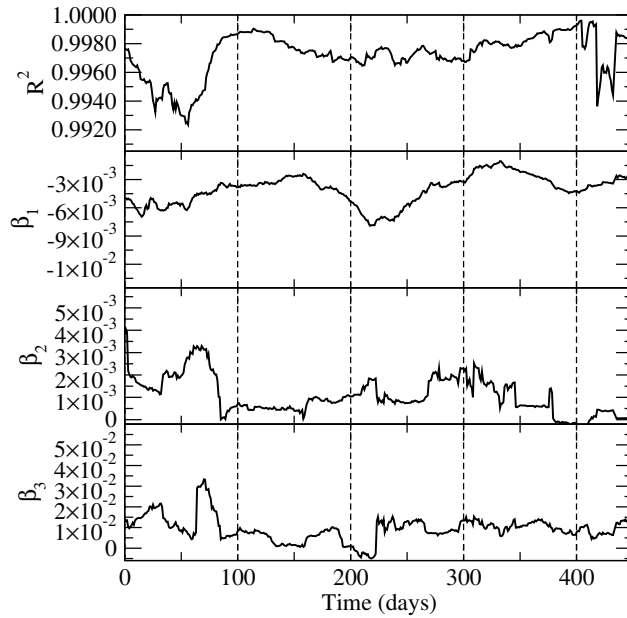


Figure 4: Time evolution of the out-of-sample performance measured by using R^2 on the first sensor of the wireless electronic nose. A window of 3 months was used to train model (5) and the next month was used to test performance. This is a forward testing methodology. The three bottom panels represent the evolution of the parameters, β_1 , β_2 and β_3 of the model over time. Note that there are seasonal changes captured in these parameters, and there is also long-term sensor drift [28].

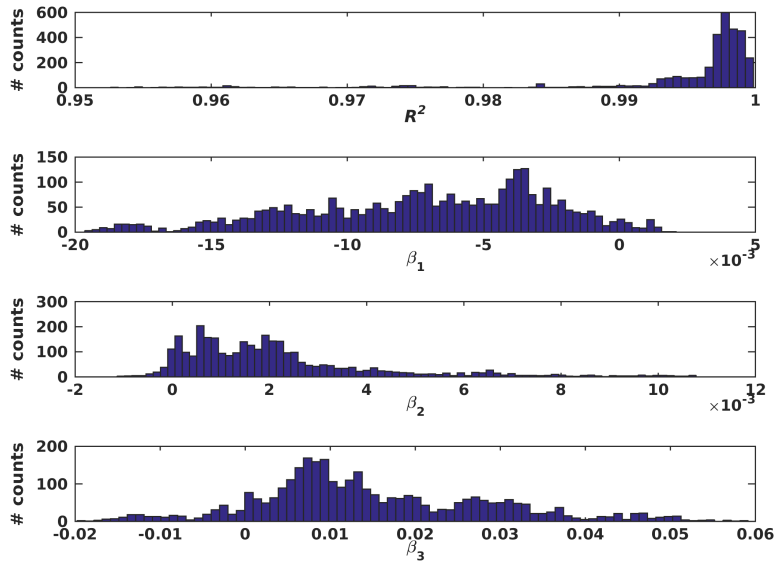


Figure 5: Histograms of the R^2 performance and the β values for all the sensors using 3 months of training and testing in the following month. It shows the model performs well despite the unstable evens that electronic noses undergo in real-time operation.

unpredictable drift in a time-scale of 6 months, as shown in [28]. In Fig. 4 we show the time evolution of the model predicting sensor values based on humidity and temperature changes. The R^2 values remain very high, staying above 0.99 threshold. The parameter values drift, reflecting environmental changes and sensor aging. Nevertheless, the band-based model is capable of adapting to these changes with only three months of historical data. To provide a more complete view of the parameter values, we also show the histogram in Fig. 5 for all the parameter values accumulated for all the sensors using the 3-month training window. The distributions tend to accumulate near the parameter values obtained in Table 2. Nevertheless, one should be aware that these parameters are expected to drift due to the natural aging processes of the sensors.

4.2 Sampling rate

The next question we want to address is what is an acceptable sampling rate on the electronic nose to be able to filter the humidity and the temperature. We estimate the effect in terms of regression accuracy of different sampling rates by computing the average R^2 values for all the sensors modifying the sampling period from 5 to 500 seconds. In Fig. 6, we can see that beyond the 2 minute sampling period the filter performance drops below 0.9. Beyond this point, the approximations made in the band based model in equations (3-4) break apart.

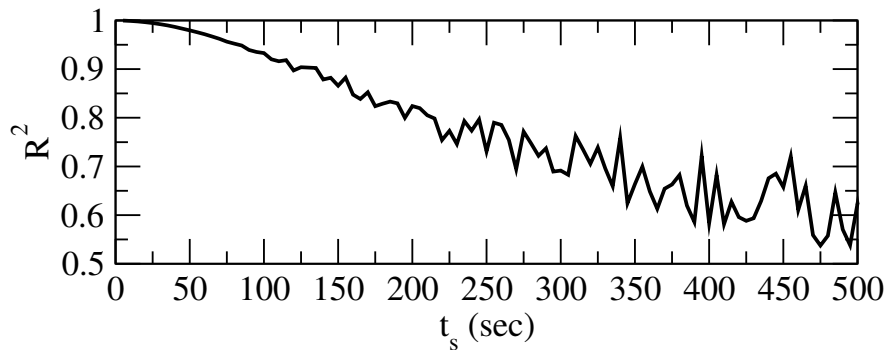


Figure 6: Average R^2 performance for increasing values of the sampling rate. Beyond the two minute sampling rate the R^2 drops below 0.9.

5 Model performance on a gas discrimination task

Over the course of two months, we collected data from the sensor array to distinguish between three classes of stimulus: wine, banana, and baseline. The data was collected by placing a sample of banana or wine next to the sensor array for a period ranging from 10 minutes to 1 hour. The time of the day when the stimulus was presented varied throughout the day, while no stimulus was placed at night. The dataset contains 34 banana and 36 wine presentations. The baseline examples were taken from 2PM to 3PM when home activity was very unlikely. The goal of the classifier is then to classify the time series of the sensors as banana, wine or baseline.

The sensor data was formatted as moving windows of 10 minutes for a given stimulus of duration, ΔT . If the stimulus was present for a long period of time, then we use as many training and testing examples as blocks of 10 minutes fit into the total duration of the stimulus. For example, if the odorant was present for 60 minutes, then 50 examples are used to train the classifier for a given presentation. These 10-minute windows can then be used to have a classifier operating in real time.

Since we are generating many training examples for a given presentation, special attention has to be directed towards model validation. The rule to make proper training, test, and validation sets is to choose the experiment number first to belong into training, testing or validation sets. Once the given presentation has been selected as training (test) set, then all the 10-minute segments generated for that given presentation remain as part of the training (test) set. This is important to prevent bias in model formation. For model selection, we used 4/5ths of the experimental presentations. We applied a 4-fold cross validation over the model selection data to select all the model meta-parameters. Once the meta-parameters have been selected, we retrain the model using all the model selection data and provide performance results on the remaining 1/5th of the data. To obtain sufficient statistics, we reshuffle the presentations and repeat this procedure 50 times.

The main question we want to address is to determine whether the classifier can potentially benefit from filtering temperature and humidity. With this purpose in mind, we test 4 different feature vector sets: raw sensor time series (RS), raw sensor data with humidity and temperature (RS+TH), filtered sensor data only (FS), and finally raw sensor data with filtered sensor data (RS+FS). To solve the classification problem we will use a nonlinear classifier that is called inhibitory SVM classifier that is Bayes consistent [29] for three classes in contrast to other multi-

Input type	Cross-validated accuracy	Accuracy in test	Std	p-value
RS	78.5%	76.5%	6.8%	0.02*
RS+TH	73.3%	71.1%	6.8%	$1 \cdot 10^{-12**}$
FS	72.4%	71.2%	4.8%	$2 \cdot 10^{-12**}$
RS+FS	82.6%	80.9%	6.3%	1

Table 3: Accuracy results of a nonlinear classifier applied to a data set of 100 examples of three classes: wine, banana and baseline activity. The first column contains the feature set: RS=raw sensor data; RS+TH= Raw sensor with temperature and humidity, FS=The sensor data after filtering with the humidity and temperature model given in equation 5; and RS+FS= Raw sensor data + filtered sensors. The accuracy in the test set is calculated after the cross-validation has selected the best meta-parameters in the training set. The value is the average of 50 random partitions of the data. The fourth column represents the p-value of a Kolmogorov-Smirnoff test of the model using RS+FS versus the rest (** passes at 1%, * passes at 5%).

class classification SVM methods using Radial Basis functions [30]. This method was successfully employed in the same sensor array in controlled conditions [31] and in wind tunnel testing [25].

The results of the multiclass classifier are presented in Table 3. The meta-parameter grid explored during the 4-fold cross-validation in the training set is $\gamma = \{0.5, 1, 5, 10, 50, 100\}$, and $C = \{10^4, 10^5, 10^6, 10^7, 10^8, 10^9\}$ (see [30, 31]) for details. After the optimal parameters were selected, the whole training data set was used to train the model with the optimal γ and C , then evaluated on the test set that was not used in the cross-validation. The raw sensors data by itself reaches good performance. Including the temperature and humidity information does not improve performance in this case, because it is providing redundant information to the classifier that is already contained in the raw sensor data. If we only use filtered sensor data then the model performs worse than the RS alone because we are losing the sensor dependencies by applying the humidity and temperature filters and we are also applying a derivative on the sensor signal. However, the model becomes very consistent (less variable in performance) compared to the one trained with the raw sensors data. The model that works significantly better using a Kolmogorov-Smirnov test is the one that combines the raw sensors data with the filtered time series. Moreover, the model consistency also improves because this configuration captures the model consistency achievable only using the filtered signal from the sensors. This example illustrates that temperature and humidity filters can not only improve pattern recognition performance but they can also improve model stability which is especially challenging in chemical sensing [32, 33, 34, 35, 36].

6 Conclusions

We used an energy band semiconductor model to express the nonlinear dependence of sensor resistance variations in an electronic nose. We found that the most dominant terms are the change in humidity, the quadratic term of the change in humidity, and the correlated variations of humidity and temperature. We showed that the model provides robust corrections to the distortions caused by environmental changes. The coefficients of determination obtained are very close to 1. The model predicts a particular dependence between two of the coefficients that is consistently verified in all the tested sensors. It is another verification that the approximations

used on the semiconductor energy band model are appropriate and an inexpensive solution for applications in continuous chemical monitoring. However, further work is still needed to consider highly ventilated scenarios in which temperature and humidity change at the same constant times than the atmosphere chemical composition.

We also showed that the maximum sampling period to obtain a reliable filter of humidity and temperature is of the order of 1 minute. The accuracy achieved with faster sampling rates provides small gains, and it would require some overhead in wireless communication when the corrections are done at the base station. Faster sampling rates may still be required to implement for some strategies that use sensor heater control in an active manner or in fast changing environments.

In order to empirically test the benefits of the humidity-temperature decorrelation model when applied to gas discrimination of the electronic nose, we built Bayes-consistent large-margin classification models to automatically detect banana, wine, and baseline in a home. Four different subsets of data were formed by combining raw sensor responses, filtered sensor data, temperature and humidity. Experimental results show that including the filtered data in the classification model improves not only the discrimination capability of the model, but, most importantly, its stability.

In summary, we have shown that electronic noses require simultaneous recordings of the humidity and the temperature to be able to isolate more relevant chemical components. Our contribution here intends to emphasize that humidity and temperature need to be simultaneously recorded and that they can be computationally embedded in sensor boards using inexpensive micro-controllers.

Acknowledgments

This work has been supported by the California Institute for Telecommunications and Information Technology (CALIT2) under Grant Number 2014CSRO 136. JF acknowledges the support of the Government of Catalonia and the COFUND programme of the Marie Curie Actions, 2013 BP-B 00190. IR-L and RH acknowledge the partial support by 3^a Convocatoria de Proyectos de Cooperacion Interuniversitaria UAM–Banco Santander con EEUU. We are also thankful to Flavia Huerta who collected data examples during the summer of 2015.

References

- [1] N. Barsan, U. Weimar, Conduction model of metal oxide gas sensors, *Journal of Electroceramics* 7 (3) (2001) 143–167.
- [2] N. Barsan, U. Weimar, Understanding the fundamental principles of metal oxide based gas sensors; the example of co sensing with SnO_2 sensors in the presence of humidity, *Journal of Physics: Condensed Matter* 15 (20) (2003) R813.
- [3] M. Hubner, C. Simion, A. Tomescu-Stanoiu, S. Pokhrel, N. Barsan, U. Weimar, Influence of humidity on $\{\text{CO}\}$ sensing with p-type CuO thick film gas sensors, *Sensors and Actuators B: Chemical* 153 (2) (2011) 347 – 353.
- [4] J. Morante, Chemical to electrical transduction mechanisms from single metal oxide nanowire measurements: response time constant analysis, *Nanotechnology* 24 (44) (2013) 444004.

- [5] M. G. Buehler, M. A. Ryan, Temperature and humidity dependence of a polymer-based gas sensor, in: *AeroSense'97*, International Society for Optics and Photonics, 1997, pp. 40–48.
- [6] N. Yamazoe, Toward innovations of gas sensor technology, *Sensors and Actuators B: Chemical* 108 (1) (2005) 2–14.
- [7] A.-C. Romain, J. Nicolas, P. Andre, In situ measurement of olfactive pollution with inorganic semiconductors: Limitations due to humidity and temperature influence, in: *Seminars in Food analysis*, Vol. 2, 1997, pp. 283–296.
- [8] F. Hossein-Babaei, V. Ghafarinia, Compensation for the drift-like terms caused by environmental fluctuations in the responses of chemoresistive gas sensors, *Sensors and Actuators B: Chemical* 143 (2) (2010) 641–648.
- [9] G. F. Fine, L. M. Cavanagh, A. Afonja, R. Binions, Metal oxide semi-conductor gas sensors in environmental monitoring, *Sensors* 10 (6) (2010) 5469–5502.
- [10] A. Oprea, J. Courbat, N. Bârsan, D. Briand, N. De Rooij, U. Weimar, Temperature, humidity and gas sensors integrated on plastic foil for low power applications, *Sensors and Actuators B: Chemical* 140 (1) (2009) 227–232.
- [11] C. Wang, L. Yin, L. Zhang, D. Xiang, R. Gao, Metal oxide gas sensors: sensitivity and influencing factors, *Sensors* 10 (3) (2010) 2088–2106.
- [12] A.-C. Romain, D. Godefroid, M. Kuske, J. Nicolas, Monitoring the exhaust air of a compost pile as a process variable with an e-nose, *Sensors and Actuators B: Chemical* 106 (1) (2005) 29–35.
- [13] A.-C. Romain, J. Delva, J. Nicolas, Complementary approaches to measure environmental odours emitted by landfill areas, *Sensors and Actuators B: Chemical* 131 (1) (2008) 18–23.
- [14] W. Bourgeois, A.-C. Romain, J. Nicolas, R. M. Stuetz, The use of sensor arrays for environmental monitoring: interests and limitations, *J. Environ. Monit.* 5 (2003) 852–860.
- [15] M. Ogawa, T. Togawa, Monitoring daily activities and behaviors at home by using brief sensors, in: *Microtechnologies in Medicine and Biology*, 1st Annual International, Conference On. 2000, IEEE, 2000, pp. 611–614.
- [16] T. Oyabu, H. Nanto, T. Onodera, Odor sensing characteristics of a lavatory in a general domicile, *Sensors and Actuators B: Chemical* 77 (1) (2001) 1–6.
- [17] T. Oyabu, A. Okada, O. Manninen, D.-D. Lee, Proposition of a survey device with odor sensors for an elderly person, *Sensors and Actuators B: Chemical* 96 (1) (2003) 239–244.
- [18] J. Fonollosa, I. Rodriguez-Lujan, A. V. Shevade, M. L. Homer, M. A. Ryan, R. Huerta, Human activity monitoring using gas sensor arrays, *Sensors and Actuators B: Chemical* 199 (2014) 398–402.
- [19] P. Chatonnet, D. Dubourdieu, Using electronic odor sensors to discriminate among oak barrel toasting levels, *Journal of agricultural and food chemistry* 47 (10) (1999) 4319–4322.

- [20] A. Shevade, M. Homer, H. Zhou, A. Jewell, A. Kisor, K. Manatt, J. Torres, J. Soler, S.-P. Yen, M. Ryan, et al., Development of the third generation jpl electronic nose for international space station technology demonstration, Tech. rep., SAE Technical Paper (2007).
- [21] M. A. Ryan, H. Zhou, M. G. Buehler, K. S. Manatt, V. S. Mowrey, S. P. Jackson, A. K. Kisor, A. V. Shevade, M. L. Homer, Monitoring space shuttle air quality using the jet propulsion laboratory electronic nose, *Sensors Journal*, IEEE 4 (3) (2004) 337–347.
- [22] A. Fort, M. Mugnaini, I. Pasquini, S. Rocchi, V. Vignoli, Modeling of the influence of h₂ o on metal oxide sensor responses to co, *Sensors and Actuators B: Chemical* 159 (1) (2011) 82–91.
- [23] R. Piedrahita, Y. Xiang, N. Masson, J. Ortega, A. Collier, Y. Jiang, K. Li, R. Dick, Q. Lv, M. Hannigan, et al., The next generation of low-cost personal air quality sensors for quantitative exposure monitoring, *Atmospheric Measurement Techniques* 7 (10) (2014) 3325–3336.
- [24] H. Windischmann, P. Mark, A model for the operation of a thin-film sno x conductance-modulation carbon monoxide sensor, *Journal of the Electrochemical Society* 126 (4) (1979) 627–633.
- [25] A. Vergara, J. Fonollosa, J. Mahiques, M. Trincavelli, N. Rulkov, R. Huerta, On the performance of gas sensor arrays in open sampling systems using inhibitory support vector machines, *Sensors and Actuators B: Chemical* 185 (2013) 462–477.
- [26] J. Fonollosa, I. Rodríguez-Luján, M. Trincavelli, A. Vergara, R. Huerta, Chemical discrimination in turbulent gas mixtures with mox sensors validated by gas chromatography-mass spectrometry, *Sensors* 14 (10) (2014) 19336–19353.
- [27] S. Cieszczyk, Sensors signal processing under influence of environmental disturbances, *Przegląd Elektrotechniczny* 4 (2013) 129–131.
- [28] A. Vergara, S. Vembu, T. Ayhan, M. A. Ryan, M. L. Homer, R. Huerta, Chemical gas sensor drift compensation using classifier ensembles, *Sensors and Actuators B: Chemical* 166 (2012) 320–329.
- [29] A. Tewari, P. L. Bartlett, On the consistency of multiclass classification methods, *The Journal of Machine Learning Research* 8 (2007) 1007–1025.
- [30] R. Huerta, S. Vembu, J. M. Amigó, T. Nowotny, C. Elkan, Inhibition in Multiclass Classification, *Neural Comput.* 24 (9) (2012) 2473–2507.
- [31] I. Rodriguez-Lujan, J. Fonollosa, A. Vergara, M. Homer, R. Huerta, On the calibration of sensor arrays for pattern recognition using the minimal number of experiments, *Chemometrics and Intelligent Laboratory Systems* 130 (2014) 123–134.
- [32] A.-C. Romain, J. Nicolas, Long term stability of metal oxide-based gas sensors for e-nose environmental applications: An overview, *Sensors and Actuators B: Chemical* 146 (2) (2010) 502–506.

- [33] M. Padilla, A. Perera, I. Montoliu, A. Chaudry, K. Persaud, S. Marco, Drift compensation of gas sensor array data by Orthogonal Signal Correction, *Chemom. Intell. Lab. Syst.* 100 (1) (2010) 28–35.
- [34] S. D. Carlo, M. Falasconi, E. Sánchez, A. Scionti, G. Squillero, A. P. Tonda, Increasing pattern recognition accuracy for chemical sensing by evolutionary based drift compensation., *Pattern Recognit. Lett.* 32 (13) (2011) 1594–1603.
- [35] A. Vergara, S. Vembu, T. Ayhan, M. A. Ryan, M. L. Homer, R. Huerta, Chemical gas sensor drift compensation using classifier ensembles, *Sens. Actuators, B.* 166–167 (2012) 320–329.
- [36] E. Martinelli, G. Magna, S. De Vito, R. Di Fuccio, G. Di Francia, A. Vergara, C. Di Natale, An adaptive classification model based on the artificial immune system for chemical sensor drift mitigation, *Sensors and Actuators B: Chemical* 177 (2013) 1017–1026.